Structural, electronic, and magnetic properties of Fe-Y alloys

Ch. Becker and J. Hafner
Institut für Theoretische Physik, Technische Universität Wien, Wiedner Hauptstraße 8-10, A-1040 Wien, Austria
(Received 22 February 1994)

Results of *ab initio* calculations of the structural, electronic, and magnetic properties of crystalline and amorphous Fe-Y alloys are presented. The structure of the amorphous phases is generated via a simulated molecular-dynamics quench, based on effective interatomic forces derived from tight-binding-bond theory. The results show that a pronounced chemical short-range order (preferred heterocoordination) exists at all compositions and that at short distances the local topology is similar in the crystalline and glassy phases. In the Y-rich alloys, medium-range concentration fluctuations are superposed to the local order. The investigation of the electronic structure using self-consistent spin-polarized linear muffin-tin orbital calculations confirms that the bonding properties are similar in the crystalline and amorphous phases. The crystalline compounds are ferrimagnetic, the negative Y moment is induced by a strong covalent interaction of the Y d band with the minority-spin Fe d band. Ferrimagnetism is also found in the amorphous alloys. In the Fe-rich range (more than 80 at.% Fe) competing ferro- and antiferromagnetic Fe-Fe exchange interactions lead to coexisting positive and negative Fe moments. The decrease of the magnetic moments of the Fe atoms with increasing Y content is strongly influenced by the strong coupling of the Fe spins to the Y moments—as a consequence a spontaneous Fe moment exists even at very small Fe-Fe coordination numbers. In addition the structural inhomogeneity of the Y-rich amorphous alloys leads to cluster magnetism.

I. INTRODUCTION

In the last two decades, the structural, electronic, and magnetic properties of binary alloys of Y with Fe, Co, and Ni have been studied extensively.[1] Originally, the interest in the crystalline compounds of Y with one of the magnetic 3d elements was motivated by the fact that they are prototypes for the interesting class of transition-metal-rare-earth (M-R) compounds. Investigations of the M-Y compounds allow one to study the contribution of the itinerant 3d magnetism to the magnetic properties of the M-R compounds, because the nonmagnetic Y atom is chemically similar to the trivalent R atoms but does not possess the large orbital magnetic moment and magnetic anisotropy of the R atoms.

Because of the itinerant character of 3d magnetism, the magnetic properties of M-Y compounds are strongly dependent on the crystal structure and lattice parameter. The M-rich compounds with stoichiometries $M_{17}Y_2$, M_5Y, $M_{23}Y_6$, M_3Y, and M_2Y crystallize in the $Zn_{17}Th_2$, Cu_5Ca, $Mn_{23}Th_6$, Be_3Nb, and Cu_2Mg lattices[2] with structures based on the tetrahedral close-packing principles outlined by Frank and Kasper.[3] Y-rich compounds with compositions MY, M_2Y_3, and MY_3 are found in the Co-Y and Ni-Y systems. They crystallize in structures (FeB, CrB, Ni_2Y_3, and Fe_3C types) describable in terms of a packing of trigonal-prismatic MY_6 units.[4] No Y-rich compounds exist in the Fe-Y system. Ni-Y compounds are nonmagnetic starting with Ni_5Y; the mean cobalt moment falls[5] from $1.6\mu_B$ in the pure metal to $0.5\mu_B$ in Co_3Y to zero in Co_2Y. Ni_5Y and Co_2Y exhibit an enhanced Pauli susceptibility and a magnetic moment can be induced by an applied external magnetic field. All stable Fe-Y compounds are ferromagnetic.[6] Neutron-diffraction[7] and NMR investigations[8] show that the magnetic moments are different on crystallographically inequivalent sites, demonstrating a dependence of the transition-metal moment on its local environment.

The onset of magnetism in binary alloys is better studied in the amorphous state where the composition can be varied continuously and is not restricted to a few crystalline phases with fixed stoichiometry. In amorphous Ni-Y alloys, the Ni moment disappears essentially at the same composition as in the crystalline compounds.[1] Amorphous Co_xY_{100-x} alloys show enhanced strong ferromagnetism:[1,9–12] At a given composition, the magnetic moment in the amorphous alloy is larger than for the crystalline counterpart and the moment vanishes only near $x \approx 40$. The strong ferromagnetism of a-Co-Y alloys contrasts with the behavior observed on amorphous Fe_xY_{100-x} alloys: A magnetic moment begins to appear near $x = 32$, but even at higher Fe content the alloys are not simple collinear ferromagnets. The magnetization curves at low temperature show a large high-field slope indicating that the moments are induced rather than aligned.[13] Equilibrium values of the iron moments may be deduced from ^{57}Fe Mössbauer spectroscopy.[14] The magnetic moment increases with increasing Fe content, but the values deduced from zero-field Mössbauer experiments are always significantly higher than those derived from magnetization measurements, even in the highest applied magnetic field.[13] The magnetic susceptibility shows a maximum at a temperature T_M that increases from $T_M = 18$ K near $x = 48$ to $T_M \approx 109$ K at $x = 88$, and strong hysteresis effects below a much higher temperature T_H ($T_H \approx 210$–230 K at $68 < x < 88$).[13] The susceptibility maximum and the hysteresis effects

are reminiscent of spin-glass behavior. The large difference between T_M and T_H is characteristic of short-range ferromagnetic correlations. The importance of these ferromagnetic correlations depends on the method and conditions of preparation. For example, melt-spun a-Fe_2Y has been reported as ferromagnetic[15] with a Curie temperature of $T_C \approx 270$ K (still much lower than in the corresponding crystalline compound with $T_C \approx 542$ K), whereas evaporated[16] or sputtered[13,17] samples are described as spin-glass like with a spin-freezing temperature $T_f \gtrsim T_M \approx 55$–$70$ K. This points to a strong dependence of the magnetic order on the atomic short-range order in the amorphous alloy.

The topic of the preparation dependence of the magnetic properties of a-Fe_xY_{100-x} alloys has also been discussed in some detail by Ishio *et al.*[18] From magnetization and magnetostriction measurements on melt-quenched samples, these authors deduce Curie temperatures of $T_C \approx 275$ K for $x = 80$, $T_C \approx 225$ K for $x = 60$, and $T_C \approx 38$ K for $x = 40$, i.e., considerably higher than T_H values for the sputtered alloys. The magnetic moments, however, show only little difference between melt-quenched and sputtered samples[18] — if there is a difference at all, the moments are higher for the sputtered material for $85 > x > 40$.

All data therefore point to the existence of random noncollinear magnetic structures in a-Fe_xY_{100-x} for $x \gtrsim 32$. At low iron content, part of the magnetization is field induced: In $Fe_{32}Y_{68}$ magnetization measurements point to a saturation moment of $\mu_S = 0.32\mu_B$, whereas the hyperfine-field data indicate a zero moment. For $Fe_{48}Y_{52}$, the Arrott plots (M^2 vs $\frac{H}{M}$) are linear in high field which suggests enhanced Pauli paramagnetism;[19] i.e., a homogeneous magnetization is induced by the magnetic field. At higher Fe content the field-induced contribution to the moment is negligible, and the variation of the magnetization results from the rotation of the moments in the applied field. The existence of a relatively large net magnetization shows that orientation of the spins is not entirely isotropic (speromagnetic), but shows a degree of anisotropy (asperomagnetism) that varies with composition. The extremely complex behavior of a-Fe-Y alloys also contrasts with the magnetic properties of amorphous Fe-Zr phases. In a-Fe_xZr_{100-x} noncollinear spin structures have been found for $x \geq 88$, but at lower iron content all data are consistent with weak collinear ferromagnetism.[20,21]

An evident problem is the explanation of the origin of the complex magnetic properties of the crystalline and amorphous (Fe,Co,Ni)-Y alloys. For the crystalline M-Y compounds, attempts have been made to interpret the magnetic properties on the basis of non-self-consistent band structure calculations and the Stoner-Wohlfarth theory.[22–25] However, the results of self-consistent, spin-polarized band structure calculations[26–28] [all using the augmented spherical wave (ASW) method] show that a rigid-band picture of magnetization is inappropriate. The densities of states (DOS) of the majority- and minority-spin bands are shaped differently due to differences in the covalent M-Y interactions. These covalent interactions induce a small negative moment on the Y sites so that the compounds are in reality ferrimagnets. Altogether, the local magnetic moments and their variations with density and composition are quite well described by local-spin-density (LSD) theory. The success of the LSD approach to the magnetism of crystalline M-Y alloys suggests that the complex magnetic structures of amorphous M-Y must be explained in terms of competing positive and negative exchange coupling[13] rather than in terms of random single-ion anisotropies[29] (the concept that has been successful for amorphous rare-earth alloys). However, LSD calculations are much more difficult for the amorphous than for the crystalline phases. Only for Co_2Y have attempts been made to extend the theoretical investigations to the amorphous state.[30,31] The enhanced ferromagnetism of the amorphous phase was explained in terms of a disorder-induced broadening of the electronic DOS, leading to an enhanced paramagnetic DOS at the Fermi level with a value larger than the Stoner-Wohlfarth limit for formation of a magnetic moment. So far, no attempt has been made to extend these investigations to a-Fe-Y, but for a-Fe-Zr the authors have been able to show that within LSD theory, fluctuations on the local atomic environment lead to competing ferro- and antiferromagnetic exchange interactions in the iron-rich limit.[32,33] The more complex properties of a-Fe-Y (especially at intermediate concentrations) remain a challenge.

In the present paper we present a comprehensive investigation of the structural, electronic, and magnetic properties of crystalline and amorphous Fe_xY_{100-x} alloys. Our studies are based on a molecular-dynamics modeling of the atomic structure using realistic tight-binding-bond forces[4,34] (Secs. II and III) and on self-consistent spin-polarized linear muffin-tin orbital[35,36] (LMTO) supercell calculations (Secs. IV and V) of the electronic structure and of the distribution of the local magnetic moments. Our results show that to a large extent the complex magnetic properties originate from characteristic variations in the atomic structure: In the Fe-rich region, amorphous Fe_xY_{100-x} alloys are structurally homogeneous, with a pronounced chemical and topological short-range order. Strong Fe-Fe and Fe-Y interactions lead to very compact Fe-Fe correlations and hence to competing positive and negative Fe-Fe exchange interactions. Y-rich Fe-Y glasses are structurally inhomogeneous. The strong covalent Fe-Y interaction, together with the large size difference, leads to incipient segregation of Fe and Y atoms extending over distances of about 10 Å. The morphology of this segregation is best described in terms of concentration fluctuations arising from the formation of Fe-enriched regions, rather than the formation of precipitates of a second phase. These Fe-enriched regions constitute ferromagnetic clusters, with the cluster moments being progressively aligned in a magnetic field.

II. INTERATOMIC FORCES

The interatomic potentials used in the molecular-dynamics modeling of the amorphous structure have

been calculated using a hybridized nearly-free-electron tight-binding-bond approach:[4,34] The s-electron contribution to the interatomic forces is calculated using standard pseudopotential theory;[37,38] the d-electron contribution may be written within local-density theory[39,40] in terms of a repulsive interaction containing the electrostatic, exchange-correlation, and nonorthogonality contributions to the total energy and a covalent bond energy $E_{d\text{ bond}}$ resulting from the formation of a d electron band.[41] Assuming the d orbitals in amorphous metals to be degenerate and neglecting the directionality of the d bonds, $E_{d\text{ bond}}$ can be written in a two-center orthogonal tight-binding approximation as[34,42]

$$E_{d\text{ bond}} = \frac{1}{2N} \sum_{\substack{i,j \\ i \neq j}} t_{ij}(R_{ij}) \Theta_{ij} \quad , \tag{1}$$

where t_{ij} is the transfer integral for d states centered at the sites i and j (distance R_{ij}) and Θ_{ij} the bond order counting the difference in the number of electrons in the bonding and antibonding states formed by the orbitals centered at sites i and j. Equation (1) describes only formally a pair interaction. In general the dependence of the bonding forces on the atomic environment enters via the bond order. For amorphous materials the problem is that the atomic configuration is not known *a priori*, but has to be calculated on the basis of the interatomic forces. These have to be calculated for an appropriately chosen reference system. For amorphous metals Hausleitner and Hafner[4,34,43] have shown that a Bethe lattice (where the local atomic environment is characterized by a mean coordination number and the average bond length) is a sufficiently realistic reference and allows in addition for an analytical calculation of the bond order. For all details we refer to these publications. Here we will discuss only the main physical effects determining the d-electron-mediated forces in transition-metal alloys. The character of the bonding forces is determined by (a) the difference in the position of the atomic d levels, $\Delta\epsilon_d$, in relation to the average band width $\overline{W}_d$ and (b) the filling of the d band. If $\Delta\epsilon_d$ is comparable or only slightly smaller than $\overline{W}_d$ (e.g., Cu-Y, Ni-Y, Ni-Zr, ...), then the alloy is close to the split band limit, with the lower part of the d band dominated by the "late" transition metal (Ni, Cu, ...) and the upper part dominated by the "early" transition metal (Y, Zr, ...). In this case the bond order for unlike-atom pairs is largest, and the pair forces show a strong preference for heterocoordination. This preference is most pronounced if the Fermi level falls into the pseudogap separating the two parts of the d band. If $\Delta\epsilon_d \ll \overline{W}_d$, the d electrons form a common band with little structure (e.g., Nb-Mo), and the pair forces are essentially additive or show a weak tendency to segregation. The trend through a series of $M_{35}Y_{65}$ alloys (M =Mn, Fe, Co, Ni, Cu, Zn) has recently been analyzed.[44] The Fe-Y system is a borderline case: In the Fe-rich regime characterized by broad overlapping Fe and Y bands, there are strong covalent forces for all three types of bonds (Fe-Fe, Fe-Y, Y-Y), but strongest for unlike-atom pairs [Fig. 1(a)]. It is important to emphasize that the origin of the strong unlike-atom interaction is in a covalent bonding and not in any kind of charge transfer. In the Y-rich regime, a much narrower Fe band overlaps with a very broad Y band. The Fe-Y forces are nearly unchanged, but the Y-Y bonding forces are now stronger than the Fe-Fe forces [Fig. 1(b)]. We shall see that this change has important consequences for

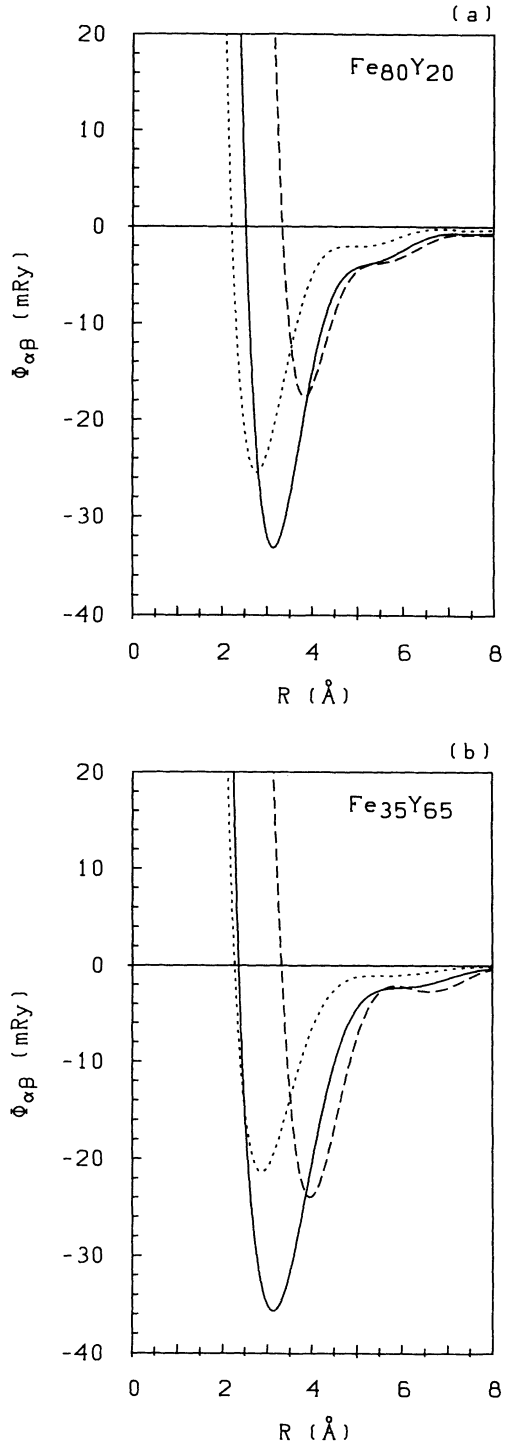

FIG. 1. Effective interatomic potentials in amorphous Fe-Y alloys [(a) $Fe_{80}Y_{20}$, (b) $Fe_{35}Y_{65}$], calculated using the hybridized nearly-free-electron tight-binding-bond approach. $\Phi_{Fe\text{-}Y}$ (solid line), $\Phi_{Y\text{-}Y}$ (dashed line), $\Phi_{Fe\text{-}Fe}$ (dotted line).

the amorphous structure. For the technical details of the calculation of the forces, we refer to Ref. 44.

III. GLASS STRUCTURE

A. Molecular-dynamics quenching

The structure of the amorphous phase has been generated by a simulated molecular-dynamics (MD) quench. The simulation is started in the liquid phase, several hundred degrees above the melting point. After reaching equilibrium, the melt is quenched to room temperature at a rate of $\dot{T} \approx 10^{14}$ K s^{-1}; technical details of the MD routines are given in Refs. 45, 46. The simulations were performed for large ensembles of $N = 1372$ atoms (serving to produce reliable correlation functions and static structure factors) and for small ensembles of $N = 64$ atoms serving to generate the coordinates for the electronic structure calculations using the supercell approach. In addition, for $Fe_{35}Y_{65}$ a simulation for a very large cell containing 10^4 atoms was performed in order to investigate medium-range concentration fluctuations (see below). Densities of amorphous Fe_xY_{100-x} alloys have been measured by Ishio *et al.*[18] and Tenhover and Duwez.[47] The experimental values agree rather well with the atomic volumes obtained on the basis of a linear interpolation of the Wigner-Seitz radii $S = (\frac{3}{4\pi}v)^{1/3}$ of the pure metals. The data are compiled in Fig. 2.

B. Pair correlation functions

Figure 3 shows the partial pair correlation functions for a selected series of amorphous Fe_xY_{100-x} alloys. The most remarkable features are (a) a strong chemical short-range order (CSRO) at all compositions, as demonstrated by the intensity of the first peak in the Fe-Y correlation function. (b) The Fe-Fe nearest-neighbor distances in the Fe-rich alloys are identical to those in pure bcc Fe

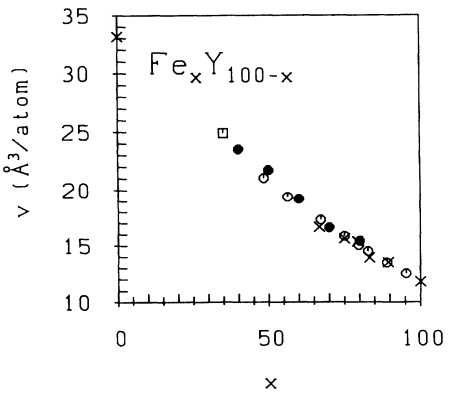

FIG. 2. Atomic volume of crystalline (×, after Ref. 2) and amorphous (□, after Ref. 18; •, after Ref. 47; ○, interpolated, cf. text) Fe-Y alloys vs composition. Volumes marked with open symbols were used in the simulations.

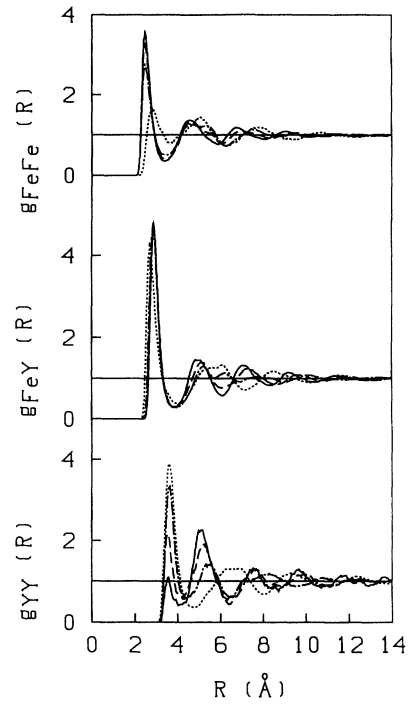

FIG. 3. Partial pair correlation functions $g_{ij}(R)$, ij = Fe,Y of amorphous Fe_xY_{100-x} alloys. $Fe_{89}Y_{11}$ (solid line), $Fe_{80}Y_{20}$ (dashed line), $Fe_{67}Y_{33}$ (dot-dashed line), $Fe_{35}Y_{65}$ (dotted line).

($d_{\text{Fe-Fe}} = 2.48$ Å); they increase up to $d_{\text{Fe-Fe}} \approx 2.75$ Å in the Y-rich alloys. The Y-Y distances ($d_{\text{Y-Y}} \approx 3.58$ Å) are compressed by 2% compared to pure hcp Y; the Fe-Y distances are smaller (by at least 7.5%) than the average distances in the pure metals. The preferred heterocoordination and the short bonds in unlike-atom pairs are the consequence of the strong covalent Fe-Y interaction (cf. Sec. II). (c) The topological short-range order (TSRO) changes with composition. This is most evident in the Y-Y correlation function. In the Fe-rich regime the ratio of next-nearest-to nearest-neighbor distance is $d_2/d_1 \lesssim 1.60$, i.e., close to the value $d_2/d_1(Cu_2Mg) = 1.633$ characteristic for the cubic (Cu_2Mg-type) Laves-phase Fe_2Y. In the Y-rich alloys, we find $d_2/d_1 \approx 1.82$, rather close to the value $d_2/d_1 \approx 1.85$ characteristic for random close packing (rcp).[48] For Fe-Fe neighbors we find $d_2/d_1 \approx 1.83$–1.85, independent of composition. This indicates that in both crystalline and amorphous Fe-rich alloys, the short-range topology conforms with the principle of a random tetrahedral close packing of large (Y) and small (Fe) atoms. In the Y-rich regime the atomic arrangement is dominated to a first approximation by the random close packing of the large Y atoms alone, with the Fe atoms filling the many holes in this structure.

C. Partial static structure factors

For a further characterization of the amorphous structure it is convenient to consider the variation of both the

Ashcroft-Langreth (AL) and the Bhatia-Thornton (BT) partial structure factors with composition (Figs. 4 and 5). The large amplitude of the first peak in the BT concentration-fluctuation structure factor $S_{CC}(Q)$ indicates again strong CSRO at all compositions. However, the character of the CSRO is different in the Fe- and Y-rich regimes. In the Fe-rich alloys, the ratio of the positions Q_{CC} and Q_{NN} of the first peaks in $S_{CC}(Q)$ and in the density-fluctuation structure factor $S_{NN}(Q)$ is $Q_{CC}/Q_{NN} \approx 0.52$–$0.64$. This value is characteristic for heterocoordination, i.e., alternant A-B bonds as in many amorphous and liquid alloys.[48] In the Y-rich alloys, the ratio increases to $Q_{CC}/Q_{NN} \approx 0.78$–$0.85$ and the position of the first peak in $S_{CC}(Q)$ is almost coincident with the first peak in the AL structure factor $S_{\text{Y-Y}}(Q)$. In parallel, the amplitude of the density-concentration structure factor $S_{NC}(Q)$ increases with increasing Y content. Both effects arise from a strong coupling between density and concentration fluctuations at a majority of the larger atoms.

In addition to the change in the SRO, the strong intensity in the small-angle region [both $S_{CC}(Q)$ and $S_{NN}(Q)$] indicates medium–range ordering in the Y-rich alloys. The inspection of the AL structure factors shows that the medium-range order (MRO) arises mainly from a redistribution of the Fe atoms. No contribution to small-angle scattering is observed in $S_{\text{Y-Y}}(Q)$ and $S_{\text{Fe-Y}}(Q)$, but $S_{\text{Fe-Fe}}(Q)$ shows a strongly increasing amplitude for $Q \leq 0.6$ Å^{-1}. A tentative interpretation is the formation of Fe-enriched regions of a characteristic dimension of $\gtrsim 10$ Å.

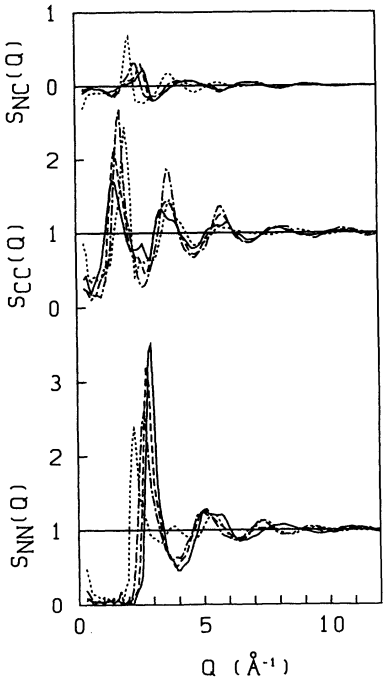

FIG. 4. Bhatia-Thornton partial static structure factors $S_{NN}(Q)$, $S_{NC}(Q)$, and $S_{CC}(Q)$ for amorphous Fe_xY_{100-x} alloys. $Fe_{89}Y_{11}$ (solid line), $Fe_{80}Y_{20}$ (dashed line), $Fe_{67}Y_{33}$ (dot-dashed line), $Fe_{35}Y_{65}$ (dotted line).

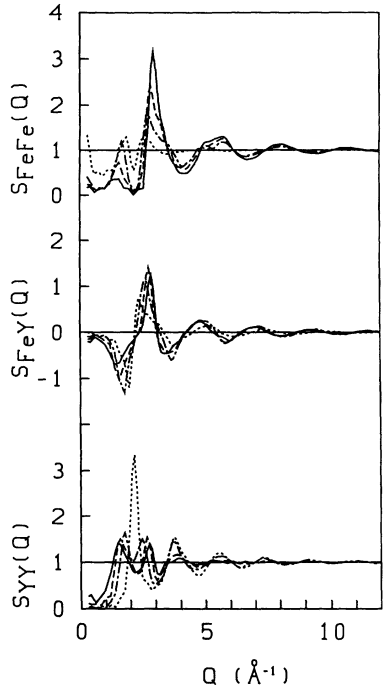

FIG. 5. Ashcroft-Langreth partial static structure factors $S_{ij}(Q)$, i,j = Fe,Y for amorphous Fe_xY_{100-x} alloys. Same symbols as Fig. 4.

D. Segregation in Y-rich amorphous Fe-Y glasses

The most direct visualization of these segregation effects can be obtained from computer graphics; Fig. 6 shows projections of slices of the quench-condensed models for several amorphous Fe_xY_{100-x} alloys (thickness 0.2 times the edge of the MD cell). Fe atoms are shown by solid, Y atoms by dotted circles. Nearest-neighbor Fe-Y bonds are drawn. One sees immediately that while the Fe-rich alloys are chemically homogeneous, the Y-rich phases show segregation in Fe-enriched and Fe-depleted regions. The characteristic diameter of the Fe-enriched regions is 8–12 Å, corresponding to the onset of small-angle scattering predicted at $Q \approx 0.6$ Å^{-1}. The tendency to segregation in Y-rich amorphous Fe-Y alloys is related to the phase diagram. All M–Y alloys with M = Mn, Fe, Co, Ni, Cu form tetrahedrally close-packed intermetallic compounds in the M-rich regime (cf. Sec. I and the discussion in Ref. 44). In the Y-rich regime, stable trigonal-prismatic compounds are formed in the Co-Y, Ni-Y, and Cu-Y systems; no stable Y-rich compounds are known in the Fe-Y and Mn-Y systems. No segregation is observed in amorphous Co-Y and Ni-Y alloys.[49]

In the Ni-Y and Cu-Y systems, the nearly full M band leads to weak M-M bonding; for the bond order we have[44] $|\Theta_{M\text{-Y}}| > |\Theta_{\text{Y-Y}}| \gg |\Theta_{M\text{-}M}|$. This is compatible with crystalline and amorphous structures based on strong M-Y and Y-Y bonds and a very small number of M-M direct neighbors. The Co-Y system shows a similar behavior, but with already somewhat stronger Co-Co bonds. In Mn-Y and Fe-Y the M band is just a little

more than half filled, and $|\Theta_{M\text{-}Y}| \approx |\Theta_{M\text{-}M}| > |\Theta_{Y\text{-}Y}|$ (see also Fig. 1). The relatively strong M-M bonding makes a structure with no M-M neighbors energetically unfavorable and leads to the formation of M-enriched regions.

The predicted formation of Fe-enriched regions is also in accordance with the observed crystallization behavior.[50] Crystallization of a-$Fe_{35}Y_{65}$ occurs in a two-step process: The first step is associated with the formation of hcp Y and an Fe-enriched amorphous phase; the second step is the formation of the Laves-phase Fe_2Y. The concentration fluctuations observed in the MD simulation may be interpreted as a precursor of the first crystallization step.

Similar segregation effects have also been reported in Fe-rich Fe-B glasses.[51] Very recently it has been shown that these segregation effects have their origin in strong covalent Fe-B interactions.[52]

E. Comparison with experiments

Early diffraction experiments[17] on a-Fe_2Y yield composite pair correlation functions in good overall agreement with the results of the present study, but only partial structure functions would constitute a critical test of the computer-generated structure. For a-$Fe_{35}Y_{65}$, Maret *et al.*[53] have made an attempt to determine a set of partial structure factors by neutron scattering and isomorphous substitution of Fe by Mn. A detailed comparison of theory and experiment has been given in Ref. 44, confirming that the computer-generated model is realistic even within details. However, it must be emphasized that the isomorphous substitution experiments are less accurate than those performed with isotopic substitution[49] on a-Ni-Y and a-Cu-Y, especially for the minority species on which the isomorphous substitution has been performed.

Segregation in a-$(Fe,Mn)_{35}Y_{65}$ has been studied by

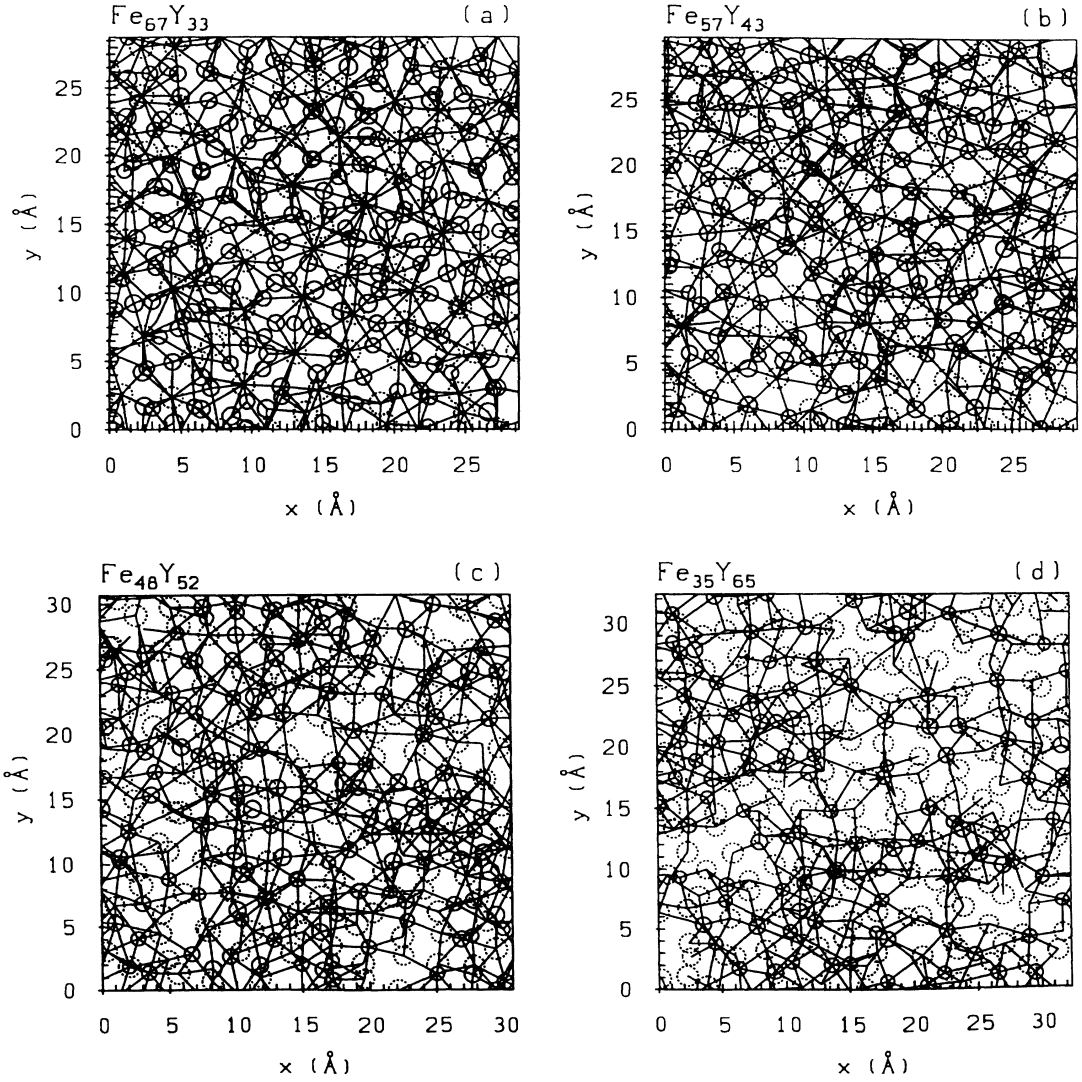

FIG. 6. Projections of slices cut out of 1372-atom models for amorphous Fe_xY_{100-x} (thickness 0.2 times the length of the MD box), projected onto the (x, y) plane. Solid circles represent Fe atoms, dotted circles Y atoms (the diameters are scaled with the z coordinate). The straight lines visualize the network of Fe-Y nearest-neighbor bonds. (a) $Fe_{67}Y_{33}$, (b) $Fe_{57}Y_{43}$, (c) $Fe_{48}Y_{52}$, (d) $Fe_{35}Y_{65}$.

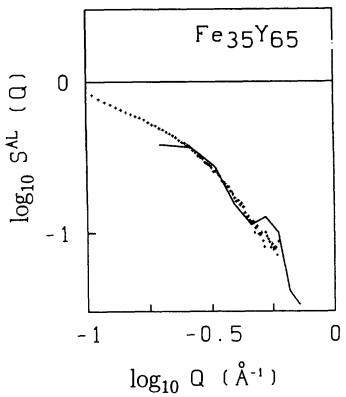

FIG. 7. Log-log plot of the small-angle x-ray scattering intensity against momentum transfer for amorphous $Fe_{35}Y_{65}$. Crosses experiment (after Ref. 54); solid line, theory.

anomalous small-angle x-ray scattering.[54] Figure 7 compares the data for a-$Fe_{35}Y_{65}$ with the present computer-generated model with 10^4 atoms. Agreement between theory and experiment is reasonable and shows that the experimentally observed long-wavelength fluctuations are well reproduced by the simulation. Maret *et al.*[54] have shown that the Q dependence of the scattering intensity may be interpreted in terms of the Ornstein-Zernike theory for microscopic concentration fluctuations with a correlation length of about 8–9 Å.

F. Summary atomic structure

Our MD-generated models lead to the following picture of the atomic structure of a-Fe_xY_{100-x}: In the Fe-rich regime we find a homogeneous amorphous structure with pronounced chemical and topological short-range order (preferred heterocoordination and random tetrahedral close packing of large and small atoms). In the Y-rich limit the structure is distinctly inhomogeneous: It is characterized by segregation into Fe-enriched regions and regions consisting of nearly pure Y. The characteristic diameter of the Fe-enriched regions is about 8–12 Å for $Fe_{35}Y_{65}$, in accordance with the correlation length for concentration fluctuations observed in small-angle scattering experiments.

IV. ELECTRONIC STRUCTURE AND MAGNETIC PROPERTIES OF CRYSTALLINE Fe-Y COMPOUNDS

The electronic structure of the crystalline Fe-Y compounds $Fe_{17}Y_2$, Fe_5Y, $Fe_{23}Y_6$, Fe_3Y, and Fe_2Y (the crystallographic data are given in Table I) has been calculated using the scalar-relativistic spin-polarized LMTO method in the atomic sphere approximation (ASA).[35,36] Exchange and correlation are described in the local-spin-density (LSD) approximation with the von Barth-Hedin[40] parametrization (using Janak's constants[55]) of the exchange correlation functional. Brillouin-zone integrations have been performed using the linear tetrahedron method with around 100 **k** points in the irreducible part of the zone. The radius ratio of the atomic spheres was chosen as $S_Y/S_{Fe} = 1.25$ for the Fe-rich alloys, near to the ratio of the interatomic distances in the Laves-phase Fe_2Y, and $S_Y/S_{Fe} = 1.35$ for $Fe_{35}Y_{65}$ to minimize the overlap between neighboring spheres.

TABLE I. Crystallographic data of Fe-Y compounds.[a]

Compound	Structure type	Pearson symbol	Lattice constants (Å)
$Fe_{17}Y_2$	$Zn_{17}Th_2$	$hR19$	$a = 8.46$ $c = 12.41$
Fe_5Y	Cu_5Ca	$hP6$	$a = 4.87$ $c = 4.06$
$Fe_{23}Y_6$	$Mn_{23}Th_6$	$cF116$	$a = 12.12$
Fe_3Y	Be_3Nb	$hR12$	$a = 5.133$ $c = 24.60$
Fe_2Y	Cu_2Mg	$cF24$	$a = 7.363$

[a]Compiled after Villars and Calvert; cf. Ref. 2.

Although the details of the electronic densities of state (Fig. 8) depend on the lattice structure, a pattern common to all compounds emerges: (a) The Fe d band is split roughly into a bonding and antibonding part. In the spin-polarized DOS, majority and minority bands are displaced such that the Fermi energy falls at the upper edge of the majority band and into the DOS minimum separating the bonding and antibonding parts of the minority band. Note, however, that for all compounds the Fermi edge lies in the majority bands so that all compounds must be classified as weak ferromagnets. (b) There are marked deviations from a rigid-band behavior; in particular the bonding-antibonding splitting is more pronounced in the DOS of the minority band. (c) Only the lower part of the broad Y d band overlaps with the Fe d band. As a consequence, the covalent Fe-Y coupling is stronger for the minority component of the Fe d band, leading to a formation of negative moments on the Y sites. Hence the Fe-Y compounds are all ferrimagnetic. Ferrimagnetism induced by covalent interactions was recently shown to be a rather common phenomenon in crystalline and amorphous inter-transition-metal[26–28,33] and transition-metal–metalloid[56,57] compounds.

The calculated magnetic moments (Fig. 9) are in good agreement with the results obtained by Coehoorn[28] using the augmented spherical wave (ASW) method and in good agreement with the experimental data from Mössbauer experiments[58–60] and neutron diffraction.[28]

The conclusion is that the weak ferrimagnetism of the crystalline Fe-Y compounds is well described on the basis of LSD calculations. The non-rigid-band behavior of the spin-polarized DOS demonstrates that these calculations must be fully self-consistent.

V. ELECTRONIC STRUCTURE AND MAGNETIC PROPERTIES OF AMORPHOUS Fe-Y COMPOUNDS

A. Supercells

Self-consistent electronic structure calculations can be performed in a supercell approximation,[61] modeling the glass by a small ensemble of atoms in a periodically repeated supercell. Using efficient band-structure codes such as the LMTO, fully self-consistent spin-polarized supercell calculations are feasible for cells containing 60–100 atoms. Attempts have been made to extend the calculations to larger cells containing several hundred atoms by transforming the LMTO Hamiltonian to a canonical tight-binding form[62] and replacing the iterative diagonalization of the Hamiltonian by a real-space recursion calculation of the local DOS and charge density. However, as the local DOS can only be calculated for a small fraction of the atomic sites, charge self-consistency can be achieved only for an average atom.[63–65] The averaging over the local charge densities may be acceptable for the calculation of spectral properties (total DOS, photoemission spectra, etc.), but as it eliminates the effects of local charge fluctuations, a fully self-consistent calculation is preferable for the investigation of local properties (e.g., the distribution of local moments). Details of the supercell technique used here have been given in our paper on amorphous (Fe, Co, Ni)-Zr alloys.[33]

Atomic configurations for the supercell calculations have been selected such that the partial pair correlation functions of a single 64-atom configuration match the

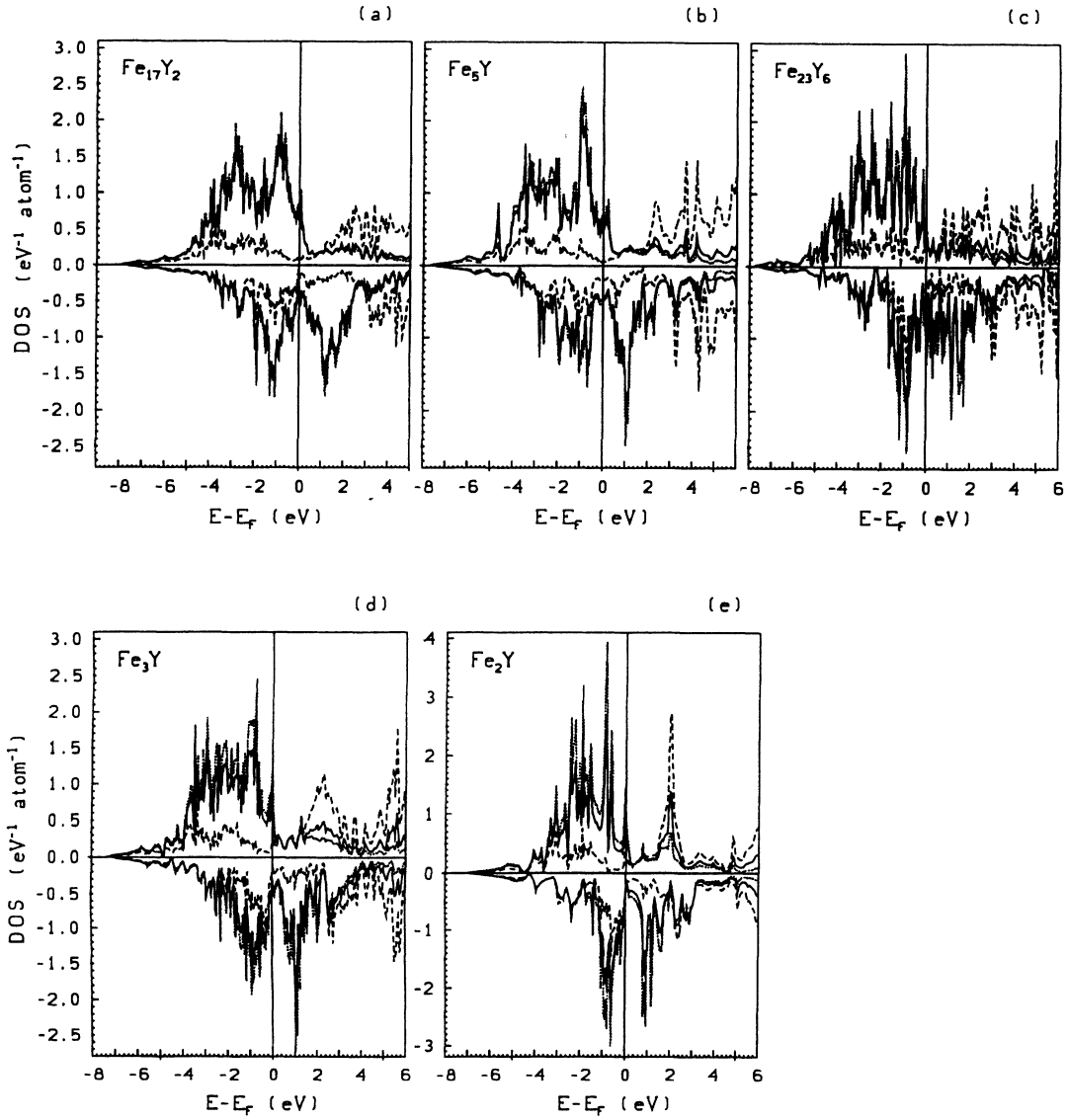

FIG. 8. Total and partial spin-polarized electronic densities of state for crystalline Fe-Y compounds. Total DOS (solid line), partial Y DOS (dashed line), partial Fe DOS (dotted line). Total and partial densities of state are normalized to the same number of atoms.

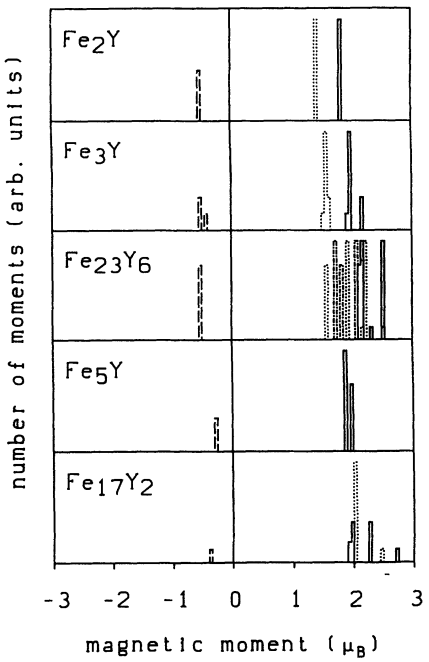

FIG. 9. Distribution of the local magnetic moments in crystalline Fe-Y compounds. Solid and dashed lines, calculated Fe and Y moments; dotted and dot-dashed lines, experimental local Fe moments from Mössbauer spectroscopy (Refs. 58–60) and neutron diffraction (cited after Ref. 28).

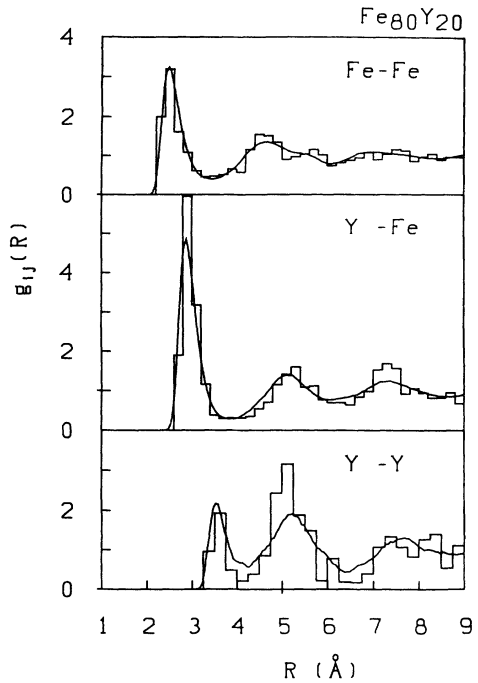

FIG. 10. Partial pair correlation functions g_{ij} for a-$Fe_{80}Y_{20}$. Histogram, a single 64-atom configuration used in the electronic structure calculations; solid line, configuration average for a 1372-atom ensemble.

configuration-averaged correlation functions of the 1372 atoms as closely as possible. An example for a-$Fe_{80}Y_{20}$ is shown in Fig. 10.

However, we should not forget to mention here a serious limitation of the supercell approach for inhomogeneous structures. For Y-rich alloys, the diameter of the 64-atom supercell is about 12 Å, i.e., of the order of the correlation length for concentration fluctuations (cf. Sec. III D). Hence the MD simulations for the small ensemble cannot fully account for concentration fluctuations on this length scale. The structures produced by the small ensembles are more homogeneous at this level, but they still reproduce the larger fluctuations in the local coordination numbers characteristic of the Y-rich alloys. This must be kept in mind when interpreting the results of the LSD calculations.

B. Total and partial densities of states

Figure 11 shows the total and partial densities of state for a series of amorphous Fe_xY_{100-x} alloys. Comparing with the crystalline DOS from Fig. 8 we note that for Fe-rich alloys in the range $90 \geq x \geq 67$ the amorphous DOS is essentially a smeared-out version of the crystalline DOS. The disorder-induced smearing affects mostly the depth of the pseudogap separating bonding and antibonding states whose depth is reduced, and much less the bandwidth and spin splitting that are essentially unaffected. As the crystalline compounds, the amorphous alloys are far from a rigid-band behavior.

In the Fe-rich limit ($x > 90$) the Fe d band is strongly broadened; the majority DOS develops a characteristic shoulder at the Fermi level. Both the broadening of the band and the DOS shoulder are the consequence of the formation of Fe sites carrying large negative magnetic moments (Fig. 12). The local DOS on the sites carrying negative moments has very much the character of an impurity DOS, with maxima at the band edges. The origin of the negative moments in terms of competing positive and negative exchange interactions will be discussed below.

The electronic DOS of the more Y-rich alloys ($x \leq 67$) is characterized by a progressive narrowing of the Fe band as a consequence of the reduced Fe-Fe coordination, and a strongly reduced bonding-antibonding splitting. For all alloys, the full width at half maximum (FWHM) of the minority band is at least 1 eV larger than for the majority band. The Fermi level falls into a DOS minimum of the majority band separating the Fe- and Y-dominated parts of the DOS. This shows that these systems are close to the transition from weak to strong ferromagnetism (but remember that the results obtained from the supercells refer to a fictitious homogeneous amorphous structure).

The electronic DOS may in principle be tested by photoemission experiments. For amorphous $M_{35}Y_{65}$ alloys (M = Mn, Fe, Ni, Cu), x-ray photoemission experiments have been performed by Tenhover *et al.*;[66] a-$Fe_{79}Y_{21}$ has been studied by Connell *et al.*[67] by photoemission and inverse photoemission. A detailed comparison between the calculated and measured $M_{35}Y_{65}$ spectra has already been given in Ref. 44, demonstrating agreement even in

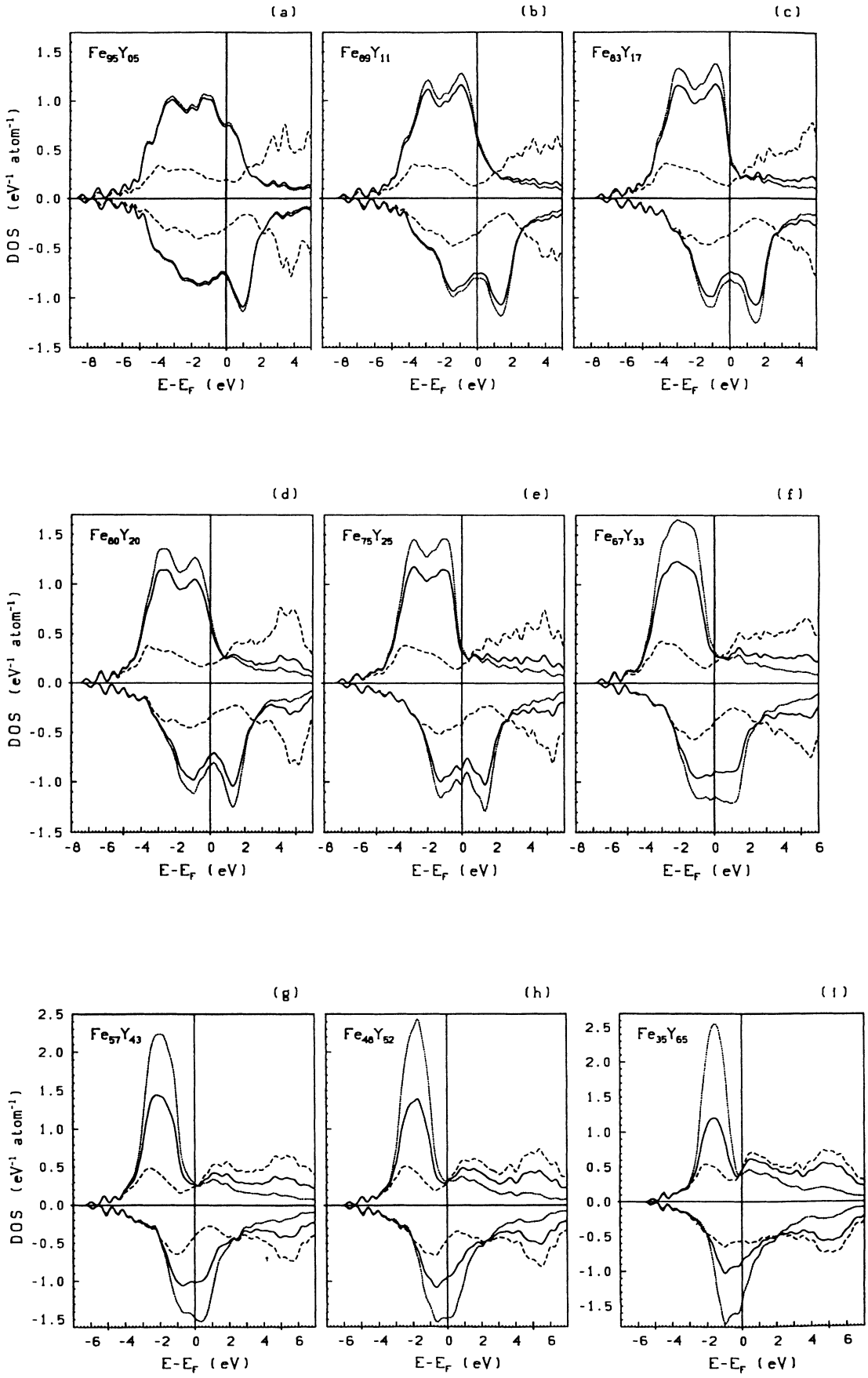

FIG. 11. Total and partial spin-polarized electronic DOS for a series of amorphous Fe_xY_{100-x} alloys. For symbols see Fig. 8.

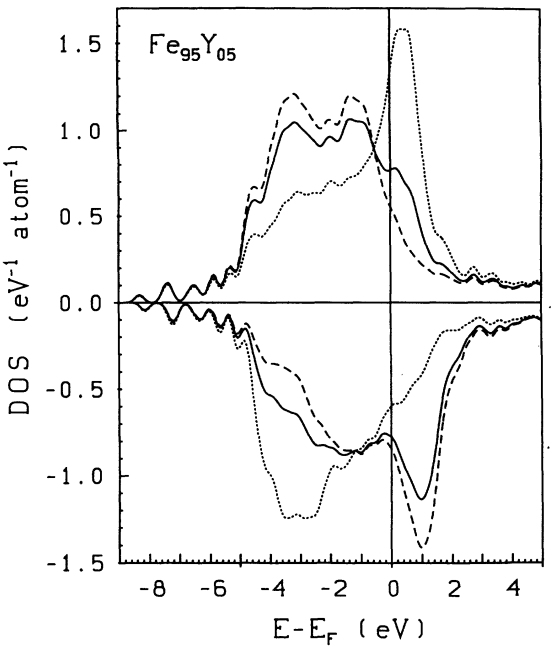

FIG. 12. Partial Fe density of states for amorphous $Fe_{95}Y_5$. The solid curve shows the Fe DOS averaged over all atoms; the dashed and dotted curves represent the average over the local DOS of the Fe sites carrying positive and negative moments respectively (44 sites with positive moment, average $1.95\mu_B$; 17 sites with negative moment, average $-1.41\mu_B$). All curves are normalized to the same number of atoms.

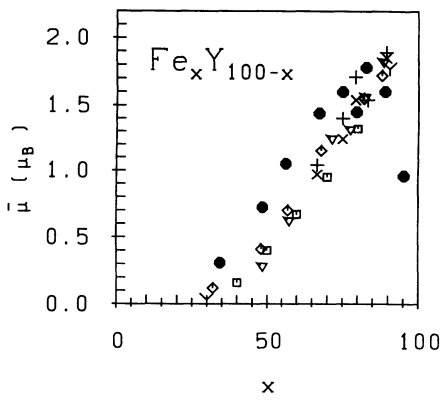

FIG. 13. Average saturation moment in crystalline and amorphous Fe-Y alloys: +, crystalline compounds, theory; × and Y, crystalline compounds, magnetization measurements (Ref. 6 and Ref. 18); •, amorphous alloys, theory; ◊ and □, amorphous alloys, magnetization measurements [Ref. 18 and Ref. 13 (extrapolated against H^{-1})]; ▽, amorphous alloys, Mössbauer experiments (Ref. 14).

details (note, however, that the room-temperature experiment refers to the paramagnetic phase of a-$Fe_{35}Y_{65}$). The uncertainty as to the magnetic state also complicates the interpretation of the experiments performed by Connell *et al.* The measurements were done on sputtered samples at room temperature; hence, according to Coey *et al.*,[13] the sample should be in a paramagnetic state. Connell *et al.* assume their sample to be ferromagnetic (which could be correct only for melt-quenched probes) and deduce a spin splitting of ≈ 1.8 eV. This would be in good agreement with the result of our LSD calculations [see Fig. 11(d)] and the predicted width of the occupied and empty parts of the d bands also agree well with experiment. However, as there are also significant differences in the calculated x-ray photoemission spectroscopy (XPS) and inverse XPS spectra, a comparison should be performed on a magnetically well characterized sample.

C. Average magnetic moment

The calculated and measured data for the average magnetic moments of all crystalline and amorphous Fe-Y phases are compiled in Fig. 13. For the crystalline compounds, the LMTO predictions are in good agreement with the magnetization data of Givord *et al.*[6] and with earlier augmented spherical wave calculations.[26–28] For the amorphous alloys, the situation is more complex. The magnetization data of Coey *et al.*[13] show no saturation, even in the highest applied fields ($H = 182$ kOe). The magnetization data in Fig. 13 refer to the saturation magnetization estimated by extrapolation against $1/H$, as proposed by Coey *et al.*[13] These estimates are always slightly below the calculated average moments. Mössbauer experiments determine the hyperfine fields at the Fe sites; magnetic moments are deduced by using a constant conversion factor of 145 μ_B^{-1} kOe, derived from the comparison of the Mössbauer data[59] and magnetization measurements[6] for the crystalline compounds. This practice assumes that only the Fe atoms carry a magnetic moment — this is evidently incorrect. Still, one might assume that the fitted conversion factor accounts for the influence of the negative Y moments in a phenomenological way. However, the negative Y moments increase from $|\mu(Y)| \approx 0.2\mu_B$ in the Fe-rich limit to $|\mu(Y)| \approx 0.4\mu_B$ around the equiatomic composition. Therefore, data on the average magnetic moment deduced from the Mössbauer hyperfine fields must be considered with some caution, especially in the concentration range where no crystalline reference data are available for fitting the conversion factor. With these caveats, the agreement between theory and experiment shown in Fig. 13 must be considered as satisfactory for the amorphous alloys as well.

The decrease of the average Fe moment with increasing Y content is usually discussed in terms of the Jaccarino-Walker model,[1] assuming that a minimum of six Fe-Fe nearest-neighbor pairs is necessary to sustain a magnetic moment on the central site. This model is not supported by the present calculations. This is easily seen by comparing the distribution of the magnetic moments in Fig. 14 with the distribution of the local Fe-Fe and Fe-Y coordination numbers given in Fig. 15. We find that as a consequence of the strong Fe-Y interactions and the CSRO induced by them, the Fe-Fe coordination decreases very rapidly, much more rapidly than the average Fe moment. Even at average Fe-Fe coordination numbers of $Z_{\text{Fe-Fe}} \approx 2$–3 (corresponding to $x \approx 35$–50),

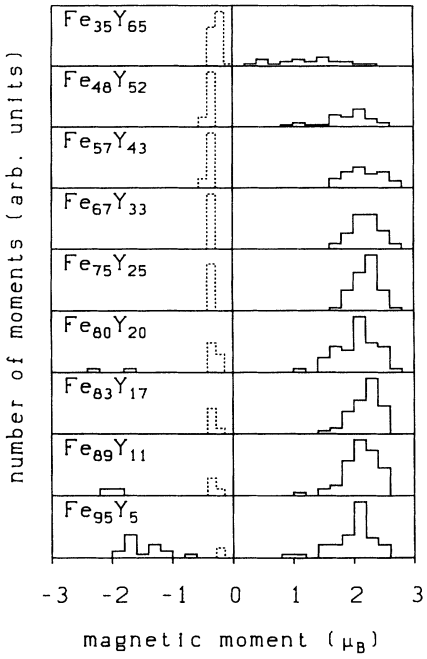

FIG. 14. Distribution of the local magnetic moments in a-Fe_xY_{100-x} alloys: Fe moments (solid line), Y moments (dotted line).

the average Fe moment is still $\mu(\mathrm{Fe}) \approx (1\text{–}2)\mu_B$. The explanation is that in contrast to, e.g., the Fe-d–B-p bonds in a-Fe-B which are only weakly polarizable, the Fe-Y bonds are highly polarizable, as shown by the relatively large moments on the Y sites. In addition to the direct ferromagnetic Fe-Fe exchange interactions, formation of Fe moments is also promoted by the ferrimagnetic Fe-Y exchange interactions induced by the strong Fe-Y covalent bond. Together with the pronounced CSRO this is equivalent to an indirect ferromagnetic Fe-Y-Fe coupling.

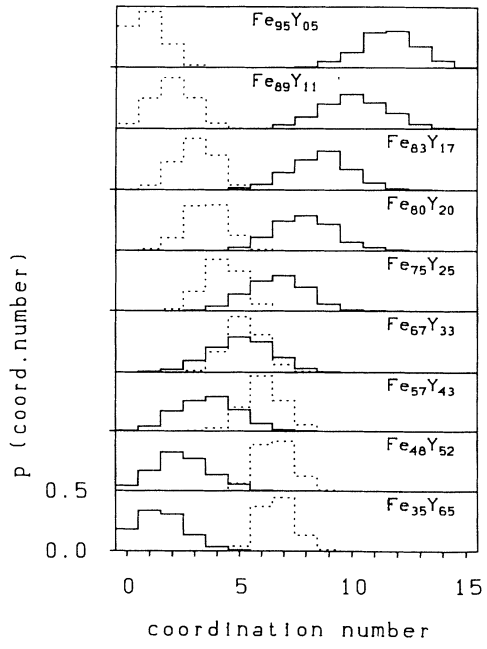

FIG. 15. Distribution of the local Fe-Fe (solid lines) and Fe-Y (dashed lines) coordination numbers in a-Fe_xY_{100-x}.

Similar criticism applies to other models that are frequently used to discuss the concentration dependence of magnetic moments in amorphous alloys, i.e., the Friedel model,[68] the hybridization-gap model of Malozemoff *et al.*,[69] and the coordination-bond model.[70] Friedel's model predicts the average moment to decrease as $\bar{\mu} = \mu(\mathrm{Fe}) - \mathrm{c}\ (10 - \delta_Z)$, where $c = (100 - x)/100$ is the atom fraction of Y and δ_Z is the host-solute valence difference ($\delta_Z = 5$ for Fe-Y alloys). With $\mu(\mathrm{Fe}) = 2.2\mu_B$ as in pure bcc iron, this predicts a much more rapid decrease of the average moment than observed experimentally — again this is due to the violation of the basic assumption that only the Fe states are polarizable, but these to the maximum extent. The assumption of fully polarizable Fe states is equivalent to assuming strong ferromagnetism, and this is as incorrect as the assumption of nonpolarizable Y states (which is also central to the coordination-bond model). The calculated DOS's for the amorphous alloys also do not show any evidence for the existence of a hybridization gap in the majority DOS at the Fermi level.

In the Fe-rich limit the calculations predict a strong decrease in the average moment. Experimentally, this region has not been explored, but a decrease of the magnetic moment with increasing Fe content has been found, experimentally[20,71] as well as theoretically,[33,57] in a-Fe_xZr_{100-x} with $x \geq 90$ and in a-Fe_xB_{100-x} with $x \geq 85$. In all cases, the decrease in the magnetic moments is due to the appearance of negative Fe moments. The results obtained here extrapolate smoothly to the moments calculated for hypothetical pure iron[32] at a density comparable to that of body-centered-cubic iron, $\mu(a\text{-Fe}) = (1.0\text{–}1.4)\mu_B$. Very recently, this prediction has been confirmed by neutron-diffraction experiments[72] on amorphous iron powders [prepared by sonochemical reduction of $Fe(CO)_5$] giving a moment of $\mu(a\text{-Fe}) = 1.4\mu_B$.

D. Distribution of magnetic moments

The distribution of the local magnetic moments in a-Fe-Y is shown in Fig. 14. Like the corresponding crystalline compounds, all the amorphous alloys are ferrimagnetic. The negative moments carried by the Y atoms are induced by the covalent interaction of the Y d states with the Fe d band, which is stronger for the Fe minority-spin band. The negative Y moments are slightly smaller in the amorphous than in the crystalline phase, but they persist even in the Y-rich range, where the alloy is close to the onset of magnetism.

For $x \leq 75$, all Fe moments are positive. Their distribution is very broad in the Y-rich alloys (e.g., ranging from $\mu \approx 0$ to $\mu \lesssim 2\mu_B$ for $Fe_{35}Y_{65}$), reflecting the fluctuations in the local environment of Fe atoms in these alloys (see Fig. 7). The distribution narrows with increasing iron content. For $x \geq 80$, a number of iron atoms acquires a negative moment. The appearance of negative moments is strongly volume dependent: This is shown in

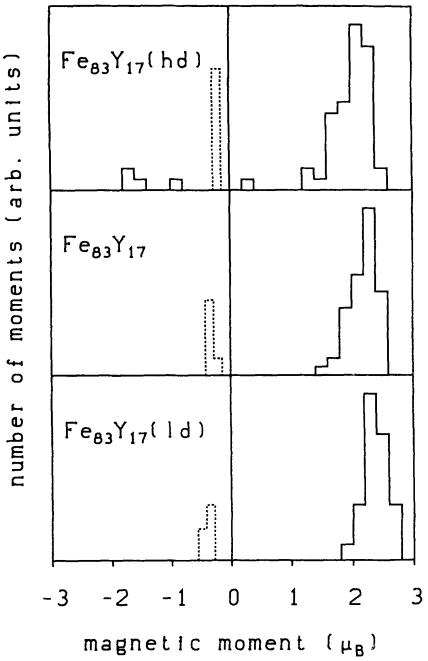

FIG. 16. Density-dependence of the distribution of magnetic moments in a-$Fe_{83}Y_{17}$, $\frac{\rho[Fe_{83}Y_{17}(ld)]}{\rho[Fe_{83}Y_{17}]} = 0.938$, $\frac{\rho[Fe_{83}Y_{17}(hd)]}{\rho[Fe_{83}Y_{17}]} = 1.037$.

Fig. 16 for the example of a-$Fe_{83}Y_{17}$. At increasing density, the distribution of the magnetic moments broadens, and a few moments align in the negative direction. In the extreme Fe-rich limit, the antiferromagnetic component of the magnetization causes a strong decrease in the average moment. The same tendency towards an increasing antiferromagnetic component in the exchange interactions has been found in our earlier work on amorphous Fe (Ref. 32) and amorphous Fe-Zr and Fe-B alloys.[33,57]

E. Competing ferro- and antiferromagnetic exchange interactions

The existence of competing ferro- and antiferromagnetic interactions in amorphous Fe-based alloys is clearly related to the transition from ferromagnetism to antiferromagnetism in face-centered-cubic and hexagonal closed-packed Fe at high density. According to LSD calculations,[73–75] this transition occurs at nearest-neighbor distances of $d \approx 2.58$ Å in fcc Fe, respectively, of $d \approx 2.63$ Å in hcp Fe. The transition from ferro- to antiferromagnetism in crystalline and amorphous systems has been discussed by Kakehashi[76] in terms of local environment effects: It is argued that a large number of "contracted" neighbors (i.e., of neighbors at short distances) leads to an antiferromagnetic polarization at the central site.

However, for the itinerant-electron magnetism of the amorphous alloys, a discussion of moment formation in terms of nearest-neighbor exchange interactions only is certainly of limited validity. Moreover, one has to remember that the formation of antiferromagnetic moments is a rather complex process: Negative moments on a given site may be stabilized by antiferromagnetic coupling to neighbors with positive moments, as well as by ferromagnetic coupling to neighbors with a negative moment. This is the reason why attempts to establish correlations between the appearance of negative Fe moments and certain types of nearest-neighbor geometries were not very successful. Nevertheless, our studies of a-Fe, a-Fe-Zr, and a-Fe-B showed that there is at least a certain correlation between negative moment and a high number of contracted neighbors,[33] in rough agreement with Kakehashi's local environment theory. Here we follow this argument somewhat further. Figure 17 shows the number of neighbors with parallel $N^p(r)$ and antiparallel $N^a(r)$ local magnetic moment as a function of distance averaged over the model for a-$Fe_{95}Y_5$. If the two curves are normalized to the same density, we find that at short distances, $N^a(r)$ is always somewhat larger than $N^p(r)$, demonstrating that indeed antiferromagnetically coupled pairs dominate at short distances.

A clearer picture arises from the examination of the local correlations. Figures 18(a,b) show the number of nearest neighbors as a function of distance for two Fe sites in a-$Fe_{95}Y_5$, one with positive moment ($\mu = 2.48\mu_B$) and one with negative moment ($\mu = -0.78\mu_B$). Around the site with positive moment, the 14 nearest neighbors are distributed evenly around the critical distance where the

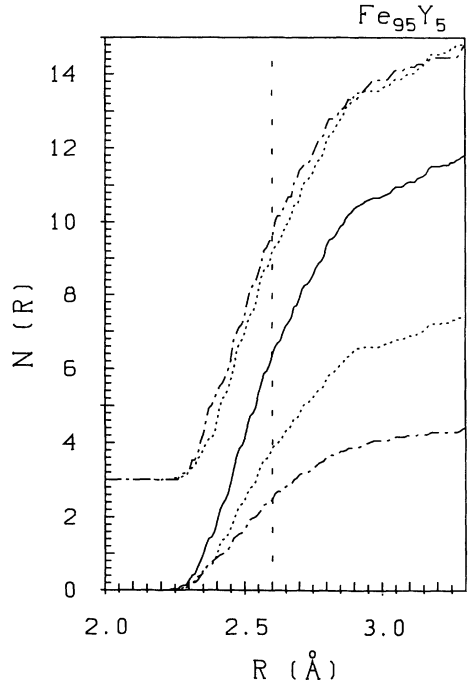

FIG. 17. Number of nearest neighbors as a function of distance in a-$Fe_{95}Y_5$. Dotted curve, pairs with parallel local magnetic moments $N^p(r)$; dot-dashed curve, pairs with antiparallel local magnetic moments $N^a(r)$; solid curve, $N(r) = N^p(r) + N^a(r)$. The two upper curves show $N^p(r)$ and $N^a(r)$ normalized to the same density and shifted by 3 for clarity. The vertical line at $r = 2.6$ Å marks the border between ferro- and antiferromagnetic exchange coupling.

exchange interaction changes sign ($d \approx 2.6$ Å). Around site 2 (with negative moment) we find eight neighbors at shorter and only three at larger distances. This is reflected already in the paramagnetic local DOS [Figs. 18(c,d)]: The predominance of short Fe-Fe distances leads to a strong bonding-antibonding splitting with a DOS at the Fermi energy of ≈ 2 states/(eV atom) at site 2. At site 1 ($\mu > 0$) we find a high local DOS at E_F [≈ 3 states/(eV atom)] and a shape of the band similar to that in bcc iron. In the spin-polarized state [Figs. 18(e,f)] majority and minority states at this site are shifted rigidly (at least in a first approximation), whereas the states at site 2 are strongly modified by spin polarization. Essentially the bonding states acquire negative spin, the antibonding states positive spin, with no shift of the characteristic peaks of the DOS. The fact

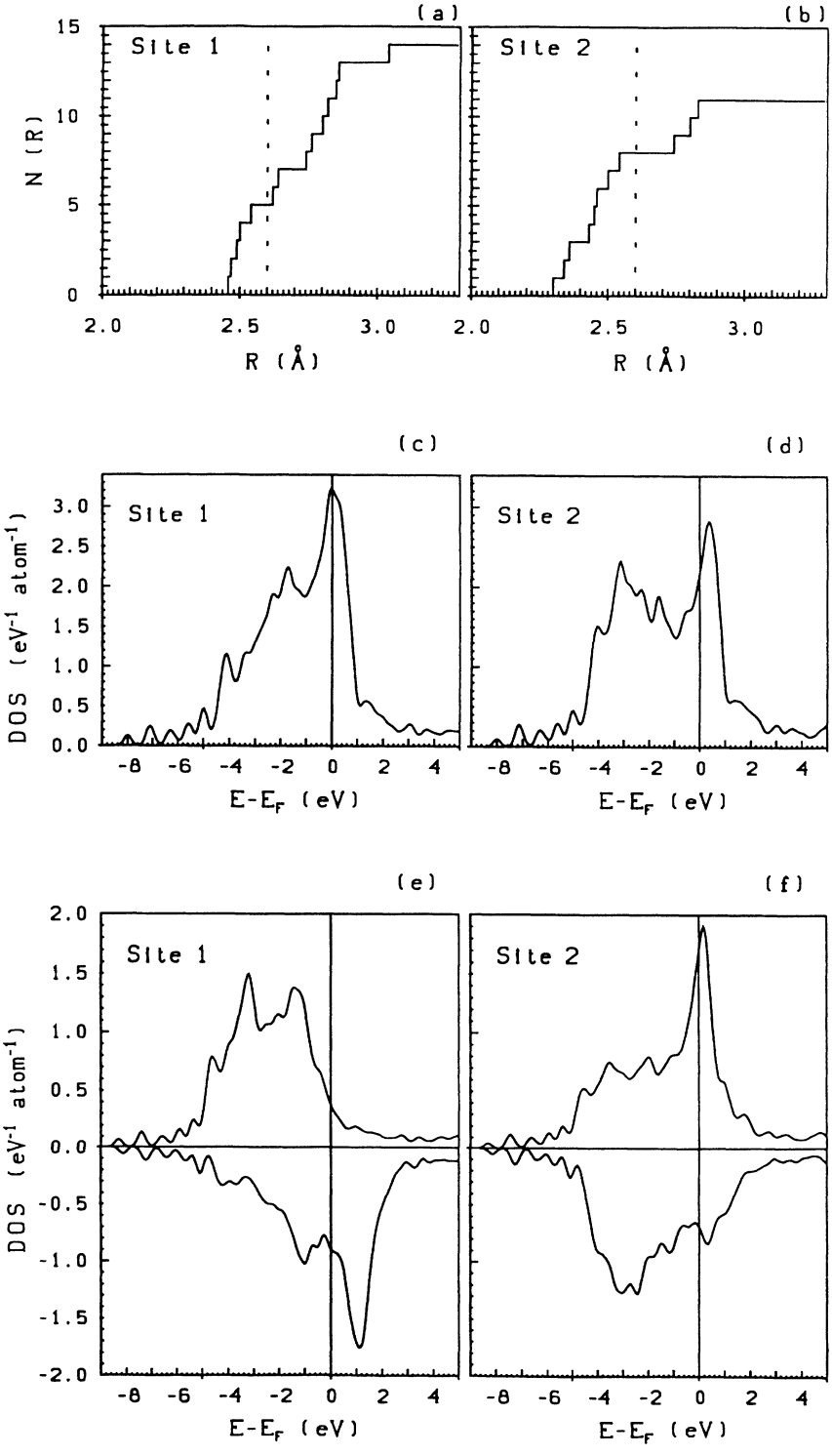

FIG. 18. (a,b) Distribution of nearest-neighbors around two sites in a-$Fe_{95}Y_5$. Site 1, $\mu_1 = 2.48\mu_B$; site 2, $\mu_2 = -0.78\mu_B$. (c,d) Paramagnetic local density of states at sites 1 and 2. (e,f) Spin-polarized local density of states at sites 1 and 2.

that sites with positive and negative moments differ already in the paramagnetic DOS shows that local charge fluctuations and local self-consistency are important for the formation of negative moments. Indeed, if we repeat the spin-polarized calculations with potential parameters averaged over the atoms of the same species [as usual in tight-binding (TB) LMTO recursion calculations[64,65]], no negative moments are found.

F. Exchange interactions

The interactions giving rise to magnetic ordering in transition-metal alloys are often described in terms of a "Stoner parameter" I. This parameter is defined by the proportionality between the exchange splitting $\Delta\epsilon$ of the d band and the magnetic moment,[77]

$$\Delta\epsilon = I\mu \quad . \tag{2}$$

In principle, this proportionality can be expected to hold only in the limit of small magnetizations (except for the case of a rigid shift of rectangular bands), but early experience with LSD calculations shows[78,79] that there is no substantial dependence of I on the degree of magnetization. This suggests treating problems of itinerant magnetism within a conventional one-electron tight-binding approximation with the additional exchange energy

$$E_{\mathrm{XC}} = -\frac{1}{4} I\mu^2 \quad . \tag{3}$$

The corresponding Hamiltonian is formally equivalent to a Hubbard model, but is to be treated strictly within the one-electron approximation, with all correlation effects assumed to be included in the effective Stoner parameter I. This maps modern LSD calculations onto the conventional Stoner picture. The question then arises whether different magnetic properties (ferromagnetism, antiferromagnetism, ferrimagnetism, spin-glass behavior, etc.) can be modeled with a single value of the constant I for a given element in different structures and alloys, and whether I changes from one element to the other. This question is particularly acute in amorphous alloys where large fluctuations in the local magnetic moments μ_i parallel large fluctuations in the local exchange splitting $\Delta\epsilon_i$. If we define the exchange splitting in terms of the center of gravity of the spin-up and spin-down bands $C_\uparrow$, $C_\downarrow$ (cf. Refs. 33, 57, 79), we find that the proportionality

$$\Delta\epsilon_i \equiv C_{\uparrow,i} - C_{\downarrow,i} = I\mu_i \tag{4}$$

holds exactly on a local level, for positive and negative iron moments as well as for the Y moments (Fig. 19). Moreover, the value $I = 0.935\mu_B/\mathrm{eV}$ deduced from the slope of the straight line fitted to Fig. 19 is exactly the same as deduced previously for a-Fe, a-Co (Ref. 32), a-(Fe,Co)-Zr alloys,[33] and a-Fe-B alloys.[57] It also agrees

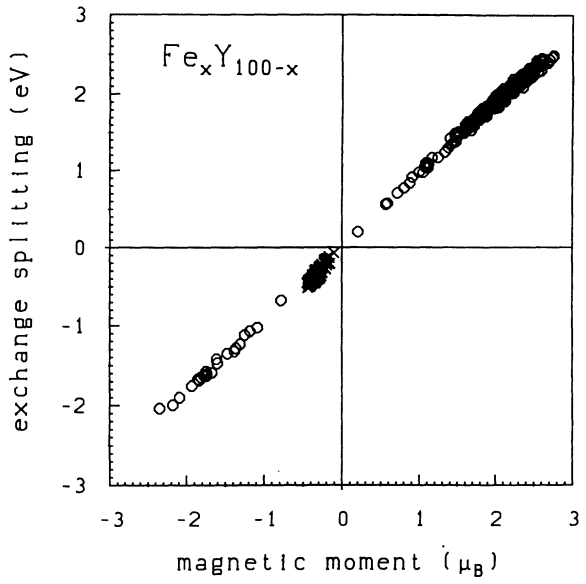

FIG. 19. Local exchange splitting $\Delta\epsilon_i$ in a-Fe$_x$Y$_{100-x}$ plotted against the local magnetic moment μ_i: ○, Fe; ×, Y.

with the value deduced recently by Himpsel[80] from the analysis of photoemission and inverse photoemission data of a wide range of ferromagnetic, antiferromagnetic, and spin-glass systems. Himpsel also pointed out that the effective I agrees with the value derived from the spin splitting and the spin moment of the free atom. This last point is important since it shows that for the itinerant d-electron magnets, the LSD Stoner parameter has to be identified with the Hund's rule exchange parameter J, as recently argued by Anisimov *et al.*[81] The constant value of the effective Stoner I then simply arises from the fact that it is an atomic property and reflects the tight-binding character of the d electrons.

The possibility to map the LSD results on a tight-binding Hubbard Hamiltonian will be important in future studies of the magnetic structure of a-Fe$_x$Y$_{100-x}$ alloys. The coexistence of exactly antiparallel iron moments distributed at random leads to a high degree of frustration and hence represents an idealized and rather unrealistic situation (in the sense that an Ising spin glass is a less realistic description of a real amorphous spin glass than a Heisenberg description). To relax the direction of the spins represents a formidable computational complication. Although attempts have been made to extend LSD calculations to noncollinear spin structures,[82,83] the application of these techniques is to date restricted to simple noncollinear structures (e.g., spin spirals) with a small number of degrees of freedom. For the $3N$ degrees of freedom in a system of N vector spins, tight-binding Hubbard techniques similar to those used by Heine and co-workers[84,85] to formulate the disordered local-moment model for transition-metal magnetism at finite temperatures seem to be more promising. Empirical TB Hubbard calculations for noncollinear spins have already been attempted by Krey and co-workers.[86] The present results show a way to base TB Hubbard calculations firmly on the results of *ab initio* LSD calculations. First results will be reported soon.[87]

VI. CONCLUSIONS

We have presented a comprehensive theoretical investigation of the structural, electronic, and magnetic properties of crystalline and amorphous Fe-Y alloys. The amorphous structure has been modeled using simulated molecular-dynamics quenches, based on effective pair interactions derived from a tight-binding-bond theory.[34] The strong interaction of the Fe and Y d states leads to strongly nonadditive pair forces at all compositions and to a pronounced chemical short-range order in the amorphous alloys. Both the chemical and the topological short-range order are very similar in the crystalline and the amorphous phases, as noted before in other M amorphous alloys.[33,4] The Fe-rich amorphous alloys are chemically homogeneous, but in the Y-rich regime the large size factor, combined with strong Fe-Y and Fe-Fe interactions, leads to concentration fluctuations on a length scale of $\gtrsim 10$ Å. These concentration fluctuations lead to the formation of Fe-enriched regions embedded in a matrix containing nearly no Fe. This clusterlike structure has a profound influence on the magnetic properties of the amorphous samples.

The local-spin-density calculations show the crystalline compounds to be ferrimagnetic, with a relatively large negative Y moment of up to $0.5\mu_B$ induced by the strong covalent interaction of the Y $4d$ band with the minority-spin band of the Fe $3d$ electrons. Our results are in good agreement with experimental values of the magnetic moments (and with previous LSD calculations[26–28]), demonstrating that the magnetism of the Fe-Y alloys has itinerant character.

The locally self-consistent LSD calculations for the amorphous alloys demonstrate a pronounced similarity of the electronic DOS of the amorphous and crystalline phases: The amorphous DOS is essentially a broadened version of the crystalline DOS (but note that the broadening increases with the Y content). This corroborates the conclusions concerning the similarity of the local structure and bonding properties drawn on the basis of the analysis of the atomic structures. It is therefore not surprising that the predicted composition dependence of the average magnetic moments of the amorphous alloys follows that of the crystalline compounds rather closely and is in reasonable agreement with experiment — except for the more Y-rich alloys where the LSD calculations tend to overestimate the saturation magnetic moment. The underlying distribution of the local magnetic moments however shows a very complex behavior: (a) All amorphous Fe-Y alloys are ferrimagnetic as the crystalline phases. (b) At Fe concentrations greater than 80 at. %, competing ferro- and antiferromagnetic exchange interactions lead to a coexistence of positive and negative Fe moments, i.e., within the limitations of collinear magnetic moments, to a spin-glass-like behavior in the Fe-rich limit. The origin of the competing exchange interactions may be traced back to fluctuations in the local environment and in local charge densities and to bonding properties. It is important that the charge densities are calculated in a locally self-consistent way — if these local charge fluctuations are eliminated by taking the average over atoms of the same species, the negative moments disappear. (c) In the direction of increasing Y content, the Fe moments decrease more slowly than suggested by simple charge-transfer or bond-breaking models. The discrepancy is the more striking, as the strong CSRO leads to a strong reduction of the number of Fe-Fe bonds. The persistence of a relatively large Fe moment in spite of Fe-Fe coordination numbers as low as 2 or 3 can only be understood if we admit the importance of indirect exchange interactions mediated by the Y atoms (note that the Y moment is almost independent of composition). The strong CSRO leads to alternant Fe-Y-Fe-Y-$\cdots$ bonds, with the Y coupling antiferromagnetically to the Fe neighbors. This leads to an effective ferromagnetic coupling of next-nearest Fe neighbors, a kind of superexchange mediated by covalent d-d interactions. (d) The 64-atom supercells on which the LSD calculations have been performed are nearly homogeneous; they are simply too small to display the medium-range concentration fluctuations characteristic for the laboratory-made samples and reproduced in larger-scale MD quenches. Therefore, the results of the LSD calculations should be considered to characterize the properties of one of the Fe-enriched clusters of diameter $\gtrsim 10$ Å, rather than those of the bulk material. With clusters of this size we estimate a cluster moment $\mu_C \approx 50\mu_B$ around equiatomic composition, in reasonable agreement with the experimental estimates.[13] Temperature and field dependence of the magnetization can be understood in terms of the alignment of the cluster moments.

In summary, our studies have shown that the structural, electronic, and magnetic properties of amorphous Fe_xY_{100-x} alloys are even more complex than the rich experimental material suggests. The structural properties are characterized by strong CSRO (induced by covalent d-d interactions), which dominates in the Fe-rich range and competes with medium-range concentration fluctuations at higher Y concentrations. The magnetic properties are characterized in the iron-rich phases by competing ferro- and antiferromagnetic exchange interactions, and in the more Y-rich phases by indirect exchange interactions mediated by the strong covalent Fe-Y bonds and by magnetic cluster effects arising from the inhomogeneity of the samples. A completely satisfactory description of both noncollinear spin structures resulting from competing exchange interactions and cluster effects remains a challenge. For the first problem, the possibility to map the LSD results on a tight-binding Hubbard Hamiltonian opens a way to treat noncollinear spin arrangements on amorphous structures which looks rather promising.[87]

ACKNOWLEDGMENT

This work has been supported by the Austrian Ministry for Science and Research within the Material Research Program, Contract No. GZ 49.787/2-24/92.

[1] K. Moorjani and J. M. D. Coey, *Magnetic Glasses* (Elsevier, Amsterdam, 1984).
[2] P. Villars and L. D. Calvert, *Pearson's Handbook of Crystallographic Data for Intermetallic Phases*, 2nd ed. (ASM International, Materials Park, Ohio, 1991).
[3] F. C. Frank and J. S. Kasper, Acta Crystallogr. **11**, 184 (1958).
[4] Ch. Hausleitner and J. Hafner, Phys. Rev. B **45**, 128 (1992).
[5] R. Lemaire, Cobalt **33**, 201 (1966).
[6] D. Givord, F. Givord, and R. Lemaire, J. Phys. (Paris) Colloq. **32**, C1-668 (1971).
[7] E. Krén, J. Schweizer, and F. Tasset, Phys. Rev. **186**, 479 (1969).
[8] A. Oppelt and K. H. J. Buschow, Phys. Rev. B **13**, 4698 (1976).
[9] N. Heiman and N. Kazama, Phys. Rev. B **17**, 2215 (1978).
[10] K. H. J. Buschow, M. Brouha, J. W. M. Biesterbos, and A. G. Dirks, Physica B **91**, 261 (1977).
[11] K. H. J. Buschow, J. Appl. Phys. **53**, 7713 (1982).
[12] K. Fukamichi, T. Goto, and U. Mizutami, IEEE Trans. Magn. **MAG-23**, 3590 (1987).
[13] J. M. D. Coey, D. Givord, A. Liénard, and J. P. Rebouillat, J. Phys. F **11**, 2707 (1981).
[14] J. Chappert, J. M. D. Coey, A. Liénard, and J. P. Rebouillat, J. Phys. F **11**, 2727 (1981).
[15] J. J. Croat and J. F. Herbst, J. Appl. Phys. **53**, 2294 (1982).
[16] N. Heiman and N. Kazama, Phys. Rev. B **19**, 1623 (1979).
[17] D. W. Forester, N. C. Koon, J. H. Schelleng, and J. J. Rhyne, J. Appl. Phys. **50**, 7336 (1979).
[18] S. Ishio, M. Fujikura, T. Ishii, and M. Takahashi, J. Magn. Magn. Mater. **60**, 236 (1986).
[19] D. M. Edwards and E. P. Wohlfarth, Proc. R. Soc. London, Ser. A **303**, 127 (1968).
[20] D. H. Ryan, J. M. D. Coey, E. Batalla, Z. Altounian, and J. O. Ström-Olsen, Phys. Rev. B **35**, 8630 (1987).
[21] D. H. Ryan and Hong Ren, J. Appl. Phys. **69**, 5057 (1991).
[22] J. Inoue and M. Shimizu, J. Phys. F **15**, 1511 (1985).
[23] M. Shimizu, J. Inoue, and S. Nagasawa, J. Phys. F **14**, 2673 (1984).
[24] H. Yamada, J. Inoue, K. Terao, S. Kanda, and M. Shimizu, J. Phys. F **14**, 1943 (1984).
[25] S. Asano and S. Ishida, J. Phys. F **18**, 501 (1988).
[26] K. Schwarz and P. Mohn, J. Phys. F **14**, L129 (1984).
[27] P. Mohn and K. Schwarz, Physica B+C **130B**, 26 (1985).
[28] R. Coehoorn, Phys. Rev. B **39**, 13072 (1989).
[29] R. W. Cochrane, R. Harris, and M. J. Zuckerman, Phys. Rep. **48**, 1 (1978).
[30] J. Inoue and M. Shimizu, J. Phys. F **15**, 1525 (1985).
[31] M. Yu, Y. Kakehashi, and H. Tanaka, Phys. Rev. B **49**, 352 (1994); Y. Kakehashi and H. Tanaka, in *The Magnetism of Amorphous Metals and Alloys*, edited by J. A. Fernandez-Boca and W. Y. Ching (World Scientific, Singapore, 1994), Chap. 1.
[32] I. Turek and J. Hafner, Phys. Rev. B **46**, 247 (1992).
[33] I. Turek, Ch. Becker, and J. Hafner, J. Phys. Condens. Matter **4**, 7257 (1992).
[34] Ch. Hausleitner and J. Hafner, Phys. Rev. B **45**, 115 (1992).
[35] O. K. Andersen, O. Jepsen, and D. Glötzel, in *Highlights of Condensed-Matter Theory*, edited by F. Bassani, F. Fumi, and M. P. Tosi (North-Holland, Amsterdam, 1985), pp. 59–176.
[36] H. L. Skriver, in *The LMTO Method*, Vol. 41 of Solid-State Sciences, edited by M. Cardona and P. Fulde (Springer, Berlin, 1984).
[37] V. Heine and D. Weaire, in *Solid State Physics*, edited by H. Ehrenreich, F. Seitz, and D. Turnbull (Academic, New York, 1971), Vol. 24, p. 247.
[38] J. Hafner, in *From Hamiltonians to Phase Diagrams*, Vol. 70 of Solid-State Sciences, edited by M. Cardona and P. Fulde (Springer, Berlin, 1987).
[39] W. Kohn and L. J. Sham, Phys. Rev. **140**, A1133 (1965).
[40] U. von Barth and L. Hedin, J. Phys. C **5**, 1629 (1972).
[41] A. P. Sutton, M. W. Finnis, D. G. Pettifor, and Y. Ohta, J. Phys. C **21**, 35 (1988).
[42] D. G. Pettifor, in *Many-Atom Interactions in Solids*, edited by R. M. Nieminen, M. J. Puska, and M. J. Manninen (Springer, Berlin, 1990).
[43] Ch. Hausleitner and J. Hafner, Phys. Rev. B **47**, 5689 (1993).
[44] Ch. Hausleitner, M. Tegze, and J. Hafner, J. Phys. Condens. Matter **4**, 9557 (1992).
[45] A. Arnold, N. Mauser, and J. Hafner, J. Phys. Condens. Matter **1**, 965 (1989).
[46] A. Arnold and N. Mauser, Comput. Phys. Commun. **59**, 267 (1990).
[47] M. Tenhover and P. Duwez, Solid State Commun. **41**, 57 (1982).
[48] Y. Waseda, *The Structure of Non-Crystalline Materials—Liquids and Amorphous Solids* (McGraw-Hill, New York, 1980); W. van der Lugt and W. Geertsma, Can. J. Phys. **65**, 326 (1987).
[49] M. Maret, P. Chieux, P. Hicter, M. Atzmon, and W. L. Johnson, in *Rapidly Quenched Metals V*, edited by S. Steeb and H. Warlimont (Elsevier, Amsterdam, 1985), p. 521.
[50] M. Tenhover, J. Phys. F **11**, 2697 (1981).
[51] P. Lamparter and S. Steeb, J. Non-Cryst. Solids **106**, 137 (1988).
[52] Ch. Hausleitner, J. Hafner, and Ch. Becker, Phys. Rev. B **48**, 13119 (1993).
[53] M. Maret, A. Pasturel, and P. Chieux, J. Phys. F **17**, 2191 (1987).
[54] M. Maret, J. P. Simon, and O. Lyon, J. Phys. Condens. Matter **1**, 10249 (1989).
[55] J. F. Janak, Phys. Rev. B **16**, 255 (1977).
[56] M. Tegze and J. Hafner, J. Non-Cryst. Solids **156-158**, 311 (1993).
[57] J. Hafner, M. Tegze, and Ch. Becker, Phys. Rev. B **49**, 285 (1994).
[58] P. C. M. Gubbens, J. J. van Loef, and K. H. J. Buschow, J. Phys. (Paris) Colloq. **35**, C6-617 (1974).
[59] P. C. M. Gubbens, J. H. F. van Apeldorn, A. M. van der Kraan, and K. H. J. Buschow, J. Phys. F **4**, 921 (1974).
[60] A. M. van der Kraan, P. C. M. Gubbens, and K. H. J. Buschow, Phys. Status Solidi A **31**, 495 (1975).
[61] S. S. Jaswal and J. Hafner, Phys. Rev. B **38**, 7311 (1988).
[62] O. K. Andersen, O. Jepsen, and M. Söb, in *Electronic Band Stucture and Its Applications*, Lecture Notes in Physics Vol. 283, edited by M. Yussouff (Springer, Berlin, 1987), pp. 1–57.
[63] S. K. Bose, S. S. Jaswal, O. K. Andersen, and J. Hafner, Phys. Rev. B **37**, 9955 (1988).
[64] H. J. Nowak, O. K. Andersen, T. Fujiwara, O. Jepsen, and P. Vargas, Phys. Rev. B **44**, 3577 (1991).
[65] A. M. Bratkovsky and A. V. Smirnov, J. Phys. Condens. Matter **5**, 3203 (1993).

[66] M. Tenhover, J. Phys. F **10**, L293 (1980); M. Tenhover, D. Lukco, and W. L. Johnson, J. Non-Cryst. Solids **61+62**, 1049 (1984).
[67] G. A. N. Connell, S. J. Oh, J. Allen, and R. Allen, J. Non-Cryst. Solids **61+62**, 1061 (1984).
[68] J. Friedel, in *Metallic Solid Solutions*, edited by J. Friedel and A. Guinier (Benjamin, New York, 1963).
[69] A. P. Malozemoff, A. R. Williams, K. Terakura, V. L. Moruzzi, and K. Fukamichi, J. Magn. Magn. Mater. **35**, 192 (1983).
[70] B. W. Corb, R. C. O'Handley, and N. J. Grant, Phys. Rev. B **27**, 636 (1983).
[71] B. Bayreuther, G. Enders, H. Hoffmann, U. Korndörfer, W. Oestreicher, K. Röll, and M. Takahashi, J. Magn. Magn. Mater. **31-34**, 1535 (1983); Ze Xianyu, Y. Ishikawa, T. Fukunaga, and N. Watanabe, J. Phys. F **15**, 1799 (1985).
[72] R. Bellissent, G. Galli, M. W. Grinstaff, P. Migliardo, and K. S. Suslick, Phys. Rev. B **48**, 15797 (1993).
[73] C. S. Wang, B. M. Klein, and H. Krakauer, Phys. Rev. Lett. **54**, 1852 (1985).
[74] V. L. Moruzzi, P. M. Marcus, and J. Kübler, Phys. Rev. B **39**, 6957 (1989).
[75] J. Kübler, Solid State Commun. **72**, 631 (1989).
[76] Y. Kakehashi, Phys. Rev. B **43**, 10820 (1991), and references therein.
[77] E. C. Stoner, Proc. R. Soc. London, Ser. A **165**, 372 (1938); E. P. Wohlfarth, *ibid.* **195**, 434 (1949).
[78] O. Gunnarson, J. Phys. F **6**, 587 (1976).
[79] U. K. Poulsen, J. Kollar, and O. K. Andersen, J. Phys. F **6**, L241 (1976).
[80] F. J. Himpsel, Phys. Rev. Lett. **67**, 2363 (1991).
[81] V. I. Anisimov, J. Zaanen, and O. K. Andersen, Phys. Rev. B **44**, 943 (1991).
[82] J. Kübler, K.-H. Höck, J. Sticht, and A. R. Williams, J. Appl. Phys. **63**, 3482 (1988).
[83] O. N. Mryasov, A. I. Liechtenstein, L. M. Sandratskii, and V. A. Gubanov, J. Phys. Condens. Matter **3**, 7683 (1991).
[84] V. Heine, J. H. Samson, and C. M. M. Nex, J. Phys. F **11**, 2645 (1981).
[85] M. U. Luchini and V. Heine, J. Phys. Condens. Matter **1**, 8961 (1989).
[86] U. Krey, U. Krauss, and S. Krompiewski, J. Magn. Magn. Mater. **103**, 37 (1992).
[87] R. Lorenz and J. Hafner (unpublished).

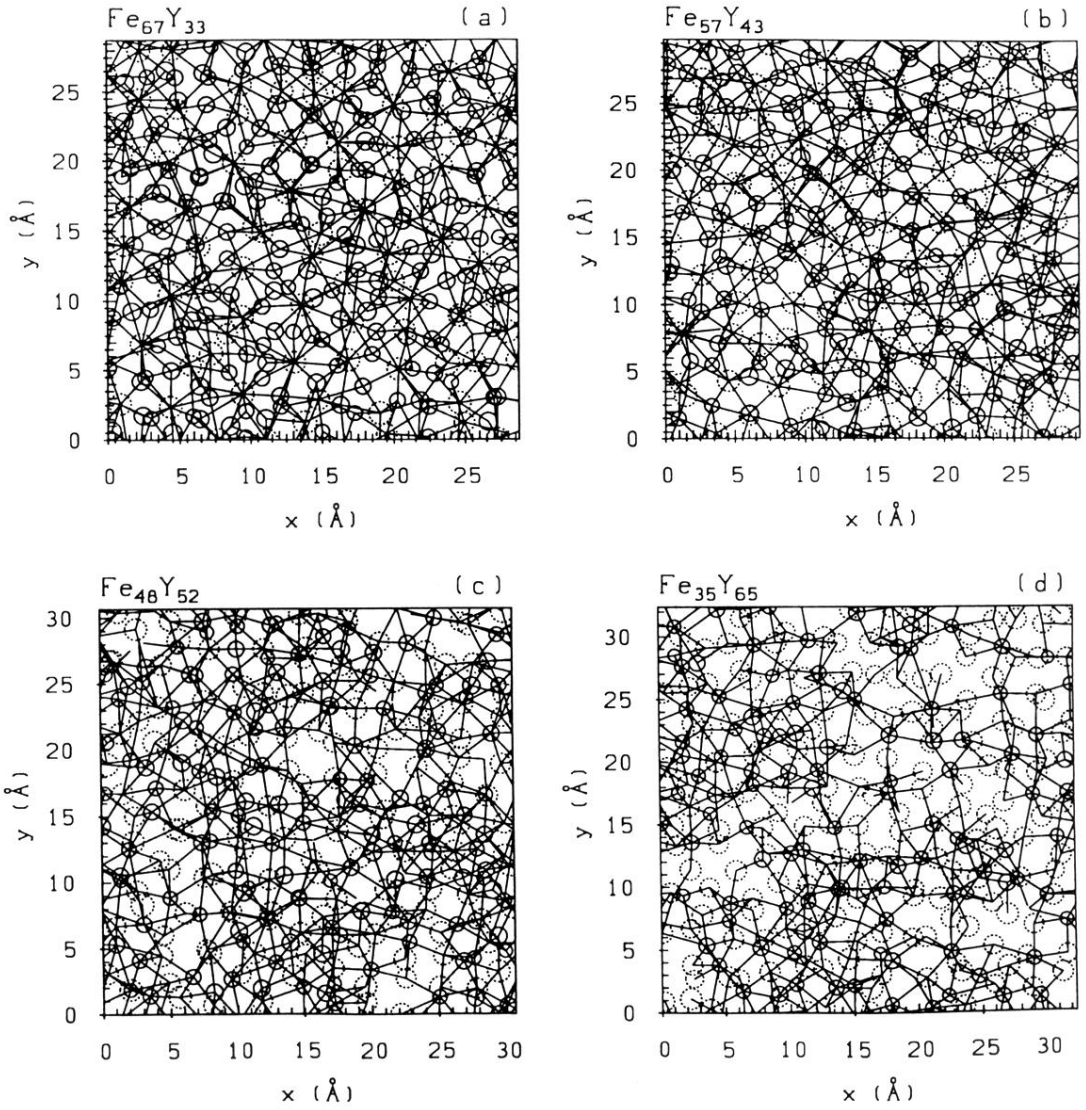

FIG. 6. Projections of slices cut out of 1372-atom models for amorphous Fe_xY_{100-x} (thickness 0.2 times the length of the MD box), projected onto the (x, y) plane. Solid circles represent Fe atoms, dotted circles Y atoms (the diameters are scaled with the z coordinate). The straight lines visualize the network of Fe-Y nearest-neighbor bonds. (a) $Fe_{67}Y_{33}$, (b) $Fe_{57}Y_{43}$, (c) $Fe_{48}Y_{52}$, (d) $Fe_{35}Y_{65}$.